Front. Optoelectron. 2016, 9(1): 81–86
DOI 10.1007/s12200-016-0573-8

RESEARCH ARTICLE

Challenges in the ambient Raman spectroscopy characterization of methylammonium lead triiodide perovskite thin films

Yuanyuan ZHOU (✉), Hector F. GARCES, Nitin P. PADTURE (✉)

School of Engineering, Brown University, Providence RI 02912, USA

Abstract The importance of methylammonium lead triiodide ($CH_3NH_3PbI_3$ or $MAPbI_3$) organic-inorganic hybrid perovskites has shot up dramatically since their use in highly efficient thin-film perovskite solar cells (PSCs). However, the basic structural characterization of these fascinating materials remains sparse. In particular, Raman spectroscopy, which is a powerful vibrational spectroscopy characterization tool and complements other characterization methods, of $MAPbI_3$ under ambient conditions is plagued with difficulties. Here, a systematic ambient Raman spectroscopy characterization study of $MAPbI_3$ thin films is conducted under different conditions (excitation laser wavelength, integration time, filter characteristic). The results from this study help elucidate the possible sources of artifacts in the Raman spectra, and raise the awareness of the challenges in the ambient Raman spectroscopy of $MAPbI_3$ perovskites. Approaches to overcome these challenges are suggested.

Keywords perovskite, solar cells, Raman spectroscopy, laser-degradation

1 Introduction

Organometal trihalide organic-inorganic hybrid perovskites with general formula ABX_3, where the "A" site is an organic-molecule cation, were first discovered in 1978 [1,2]. The structural understanding, solution-processing, and properties of this remarkable family of materials were further developed in the 1990s [3], but their use in solar cells in 2009 [4] has sparked tremendous interest in these hybrid organic-inorganic materials for photovoltaics [5–13], and also other applications [14–17]. The most popular and the most well-studied perosvkite is methylammonium lead triiodide ($CH_3NH_3PbI_3$ or $MAPbI_3$). This is primarily because of the relative ease by which high-quality thin films of $MAPbI_3$ can be deposited using a variety of solution-based techniques [18–20], and the high power conversion efficiencies (PCEs) that can be obtained in perovskite solar cells (PSCs) based on thin films of $MAPbI_3$ [10–13]. While $MAPbI_3$ perovskite has been characterized extensively using a battery of analytical methods, there is relatively little effort on its Raman spectroscopy in the open literature [21–25]. Raman spectroscopy is a very powerful and sensitive vibrational spectroscopy characterization tool for gaining insight into the structure of materials, in particular organic-inorganic hybrid materials like $MAPbI_3$ perovskite, and complements other characterization tools such as infrared (IR) spectroscopy, X-ray diffraction (XRD), and nuclear magnetic resonance (NMR) [26]. Strong Raman signal can be obtained from small volume of material, making it highly sensitive [26]. Also, Raman signal is sensitive to strain, which can be used to measure the stress state in the material [26].

$MAPbI_3$ crystallizes in tetragonal perovskite structure under ambient conditions (Fig. 1) [27,28] because its Goldschmidt tolerance factor, t, is less than the ideal unity (t~0.83) [3,29]:

$$t = [(r_{MA^+}) + (r_{I^-})]/[\sqrt{2}(r_{Pb^{2+}}) + (r_{I^-})], \qquad (1)$$

where r is the respective ionic radii. The space group I4/mcm indicates $a^0a^0c^-$ (Glazer notation [30]) PbI_6-octahedra tilting (one-tilt) in $MAPbI_3$ to accommodate the non-ideal t. Furthermore, the presence of the polar MA^+ cation in the PbI_6-octahedra "cage" could result in the loss of inversion symmetry in $MAPbI_3$ at room temperature [27]. While experimental Raman spectra of $MAPbBr_3$ [31] and $MAPbCl_3$ [32] perovskites under ambient conditions have been reported in the literature,

Received December 17, 2015; accepted December 31, 2015

E-mails: yuanyuan_zhou@brown.edu, nitin_padture@brown.edu

ambient Raman scattering from $MAPbI_3$ perovskite has not been studied until very recently. However, there are significant discrepancies between the reported Raman spectra of $MAPbI_3$ perovskite [21,22,24,25]. This has motivated us to perform systematic Raman spectroscopy experiments on $MAPbI_3$ perovskite thin films in the ambient to investigate the possible sources of these discrepancies.

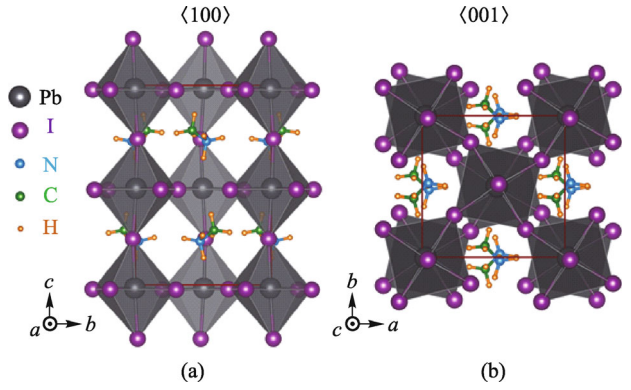

Fig. 1 Crystal structure of $MAPbI_3$ perovskite: (a) ⟨100⟩ view and (b) ⟨001⟩ view

2 Experimental procedure

A smooth 100-nm thickness Al layer was deposited on quartz plates using electron beam deposition (Lesker Laboratory 18, Kurt Lesker, USA), which constitutes the substrates. Standard $MAPbI_3$ thin film with smooth, full-coverage morphology was then deposited on the substrates using a method reported elsewhere [33,34]. Briefly, 40 wt% precursor solution of MAI (Dyesol, Australia) and PbI_2 (Acros Organics, USA) (MAI:PbI_2 = 1:1, molar ratio) was dissolved in a mixed solvent of 1-N-methyl-2-pyrrolidinone (NMP)/γ-butyrolactone (GBL) (7:3, weight ratio). The precursor solution was then spin-coated on the Al-coated quartz substrates by spin-coating at 4500 r/min for 10 s. The solution-coated substrate was then dipped into a stirring diethyl ether (Fisher Scientific, USA) bath for 2 min. The as-crystallized dark film was then taken out of the bath and rapidly dried using nitrogen, and annealed at 100°C for 5 min in a nitrogen-fill glovebox (< 0.1 ppm[1] H_2O). The freshly-made film were characterized immediately.

The as-prepared $MAPbI_3$ thin films were characterized using XRD (Bruker D-8 Discover, Karlsruhe, Germany) with Cu $K\alpha_1$ radiation (λ = 1.5406 Å) at a step size of 0.02°. The surface and cross-sections (fractured) morphology of the as-prepare $MAPbI_3$ thin films were characterized using a scanning electron microscope (SEM; LEO 1530VP, Carl Zeiss, Germany).

A confocal Raman spectrometer (Witec Alpha 300, Ulm, Germany) was used to collect Raman spectra in the ambient, using two different laser excitations: Nd:YAG 532 nm and He:Ne 633 nm. A 100× objective with a holographic grating of 600 grooves·mm^{-1} (BLZ 500 nm), and a 100 μm diameter pinhole were used. In some cases, a holographic notch-filter was used with the 532 nm laser to collect Raman spectra at low wavenumber. The laser power at the sample for the 532 nm laser without and with the low-wavenumber notch-filter was 0.61 and 0.89 mW, respectively. For the 633 nm laser power at the sample was 4.31 mW (without the low-wavenumber notch-filter). All Raman measurements were performed under ambient conditions (~20°C, ~30% relative humidity (RH)).

3 Results and discussion

Figure 2(a) shows indexed XRD pattern of the as-prepared $MAPbI_3$ thin film confirming the presence of phase-pure tetragonal $MAPbI_3$ perovskite. The location of the main PbI_2 peak is marked, confirming the absence of PbI_2 within the resolution of the XRD [35]. The phase-purity of the $MAPbI_3$ thin film is of particular importance, primarily because the precursor (MAI and PbI_2) phases are Raman active, which will be discussed later. The top-view and cross-section SEM images in Figs. 2(b) and 2(c), respectively, show uniform coverage of the $MAPbI_3$ thin film on the substrate, indicative of a near-ideal thin-film sample characteristics. Note that the smooth Al layer of 100 nm thickness deposited on the quartz substrate prior to $MAPbI_3$ film deposition is Raman inactive (within the measured wavenumber range). This precludes any substrate-related artifacts in the Raman spectra that can occur when using other common substrates such as glass, TiO_2, ZrO_2, etc.

Since Raman scattering is inelastic, which is independent of the wavelength of the excitation monochromatic light [26], detailed Raman studies are typically carried out using two lasers with different wavelengths (e.g., 532 and 633 nm, which are readily available commercially). This helps isolate any spurious effects such as fluorescence [26]. Figures 3(a) and 3(b) are Raman spectra of as-prepared $MAPbI_3$ thin films excited with two different lasers, and at two different integration times. The right panel shows corresponding optical images of the areas before and after Raman characterization. Raman spectra of the bare Al-coated quartz substrates (short integration time: 0.2 s, 10 accumulations) are also included as reference in Figs. 3(a) and 3(b), confirming no Raman signal from the substrate in the wavenumber range of interest. Figure 3(a) shows Raman spectra with short (0.2 s, 10 accumulations) and long (2.0 s, 10 accumulations) integration times using 532 nm laser excitation (0.61 mW power). The prominent

1) 1 ppm = 1×10^{-6}

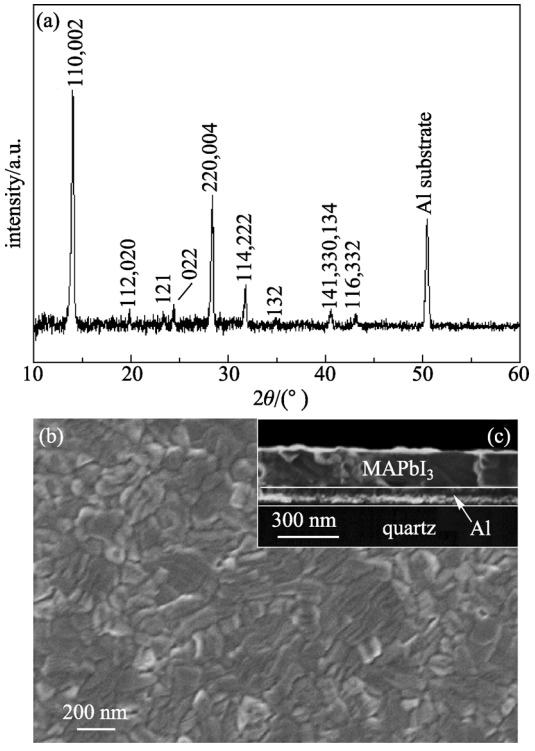

Fig. 2 Characterization of $MAPbI_3$ perovskite thin films deposited on Al substrate: (a) indexed XRD pattern, (b) top-view SEM image, and (c) cross-sectional SEM image

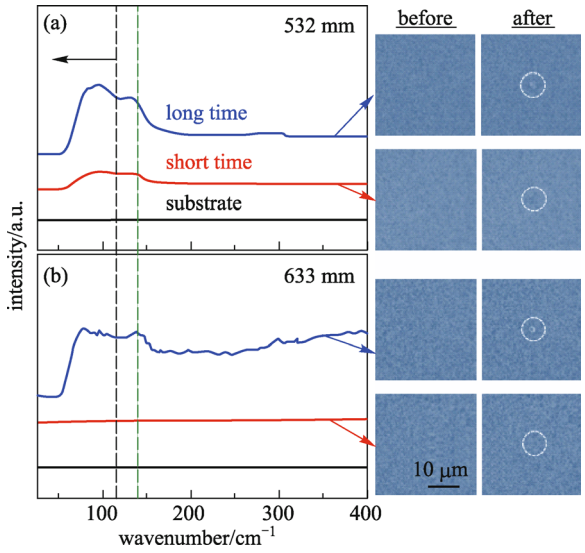

Fig. 3 Raman spectra (left) of $MAPbI_3$ thin films on Al-coated quartz substrates at short (0.2 s, 10 accumulations) and long (2.0 s, 10 accumulations) integration times (with regular notch filter), and corresponding before and after optical micrographs (right) of the sample: (a) 532 nm laser excitation, (b) 633 nm laser excitation

band around ~110 cm^{-1} in all the spectra is a spectral artifact due to the cut-off edge of the filter, which becomes more pronounced with long integration time, as expected. Note that the filter with different cut-off edges may result in such bands occurring at different wavenumbers. Besides the "filter-edge" effect, another prominent band around ~130 cm^{-1} becomes better resolved at long integration time. However, the film has been significantly damaged by the laser, as seen in the corresponding optical images in the right panel. This suggests that this evolved band in Fig. 3 (a) is primarily from degradation products of $MAPbI_3$ perovskite under the laser, and it can be the result of fluorescence and/or Raman scattering from those products. Again, such a band can also be the result of spectral artifacts, combined with signal integration, considering that it is near the filter cutoff. For Raman spectra using 633 nm laser excitation (4.31 mW power) in Fig. 3(b), similar results are obtained.

To reduce the "filter-edge" effect of the regular notch filter, a low-wavenumber holographic notch filter is used to conduct more reliable Raman spectroscopy characterization (533 nm laser excitation), and the results are presented in Fig. 4. As seen in Fig. 4, the prominent bands at ~100 and ~130 cm^{-1} that appear in Fig. 3(a) are absent, regardless of the integration time. While no observable peaks are shown in the short-integration time case, a shoulder at ~100 cm^{-1} evolves with longer integration time. However, pronounced damage to the film is observed in the optical images at long integration time in the right panel of Fig. 4. This, again, indicates that these bands may originate from the degradation products rather than the $MAPbI_3$ perovskite itself.

$MAPbI_3$ perovskite absorbs the laser radiation strongly, and it also has a low thermal conductivity (0.5 $W \cdot K^{-1} \cdot m^{-1}$) [36]. These factors can result in local heating of the film [25], which in turn is highly likely to result in the thermal decomposition of $MAPbI_3$ perovskite via $MAPbI_3 \rightarrow PbI_2 + MAI$ reaction. Thus, PbI_2 and MAI are expected to be the first degradation products. Figures 5(a) and 5(b) show typical ambient Raman spectra of PbI_2 and MAI (short integration time: 0.2 s, 10 accumulations; 532 nm laser; with low-wavelength holographic notch filter), respectively. The three main bands in PbI_2 occur at ~73, ~97, and ~112 cm^{-1} in Fig. 5(a). These are fully consistent with those observed by Khilji et al. [37] for PbI_2 at room temperature. For MAI, a major band occurs at ~114 cm^{-1} (Fig. 5(b)). The coherent anti-Stokes lines are also observed in their Raman spectra (not shown here), which suggests that those bands are indeed from Raman scattering from PbI_2 and MAI. It has been suggested that PbI_2 can degrade into Raman-active lead oxides (PbO_x) in the ambient under laser irradiation [38]. These considerations support the argument that the observed shoulder band in Fig. 3(a) (long integration time) is most likely from primary (PbI_2, MAI) and secondary (lead oxides) products of $MAPbI_3$ perovskite degradation.

While identical characterization conditions have been used for the $MAPbI_3$, PbI_2 and MAI samples (short integration time: 0.2 s, 10 accumulations; 532 nm laser;

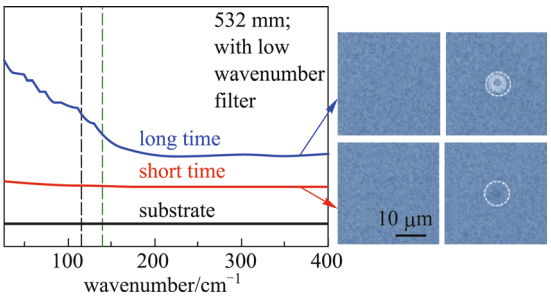

Fig. 4 Raman spectra (left) of $MAPbI_3$ thin film on Al-coated quartz substrate at short integration time (0.2 s, 10 accumulations), with low-wavelength holographic notch filter (532 nm laser excitation)

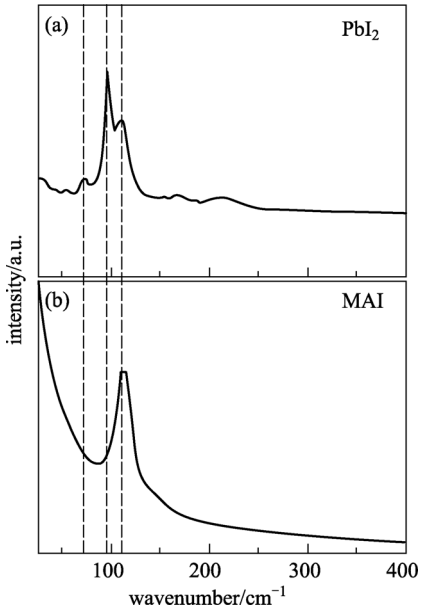

Fig. 5 Raman spectra of (a) PbI_2 and (b) MAI thin films on Al substrates: short integration time (0.2 s, 10 accumulations); 532 nm laser excitation; with low-wavelength holographic notch filter. Dashed lines mark the centers of the PbI_2 bands

with low wavelength holographic notch filter) in Figs. 4 and 5, well-resolved Raman scattering spectra have been observed only in the case of PbI_2 and MAI. This implies that significant Raman scattering under laser excitation does not occur in the $MAPbI_3$ perovskite case under ambient conditions. Note that we also conducted Raman spectroscopy on phase-pure $MAPbI_3$ perovskites (single crystals or thin films) that were deposited using other typical methods ("one-step," "two-step," solvent engineering, etc.) [10–13], with consistent results. Thus, the characterization of the relatively weak Raman scattering in $MAPbI_3$ perovskite has been highly challenging using typically available laser excitation sources. While the tradeoff between sample damage (chemical stability in the ambient under laser irradiation) and signal intensity by adjusting the integration time is well known, this tradeoff is particularly severe in the $MAPbI_3$ perovskite case — low integration time yield little to no Raman signal, while longer integration time needed for obtaining Raman signal damages the sample, and the spectra are essentially from the degradation products rather than the $MAPbI_3$ perovskite itself. This appears to be responsible for the striking variability in the Raman spectra of $MAPbI_3$ perovskite reported in the literature. To circumvent this issue, Ledinský et al. [25] used a 785 nm laser, but still found damage to $MAPbI_3$ perovskite at room temperature. Brivio et al. [23] also used a 785 nm laser, but they were able to perform their Raman experiments on $MAPbI_3$ perovskite only at 100 K (orthorhombic phase), where they found no damage. Ledinský et al. [25] have suggested that the optimal laser wavelength is 830 nm, which is above the absorption edge and peak photoluminescence (PL) in $MAPbI_3$ perovskite. Unfortunately, such long-wavelength lasers are not readily available commercially. While one can experiment with power and integration time parameters using conventional excitation lasers used in commercial Raman spectrometers, questions will remain regarding the validity of those measurements. Thus, to remove any ambiguity regarding the Raman results for $MAPbI_3$ perovskites under ambient conditions, it is imperative that infrared ($>$ 830 nm wavelength) excitation lasers must be used in the future.

4 Conclusion

A systematic ambient Raman spectroscopy characterization study of $MAPbI_3$ thin films is conducted by varying the excitation laser wavelength, integration time, and filter characteristics. The comprehensive results, which are obtained using available characterization resources, indicate that Raman scattering under laser excitation under ambient conditions from $MAPbI_3$ perovskite is insignificant compared to that from the precursor phases and/or degradation products (MAI, PbI_2, PbO_x, etc.). This does not exclude the possibility of the existence of the weak Raman scattering in $MAPbI_3$ perovskite. It is found that the use of typically available laser excitation sources (532 and 633 nm) easily damages the $MAPbI_3$ thin films, and resulting Raman spectra contain spectral artifacts and bands from Raman scattering by primary (PbI_2, MAI) and secondary (lead oxides) degradation products rather than the $MAPbI_3$ perovskite itself. This becomes a challenging issue in the ambient Raman characterization of $MAPbI_3$ perovskite, and it is likely to be the source of the discrepancies found in the Raman spectra of $MAPbI_3$ perovskite reported in the literature. This challenge may be overcome by using the less common infrared ($>$ 830 nm wavelength) excitation lasers. The lessons learnt from this Raman spectroscopy studies of $MAPbI_3$ perovskite can be

extended to other laser-sensitive light-absorbing compounds such as $CsSnI_3$, $HC(NH_2)_2PbI_3$, etc.

Acknowledgements Research support from the National Science Foundation (award nos. DMR-1305913, OIA-1538893) is gratefully acknowledged.

References

1. Weber D. $CH_3NH_3SnBr_xI_{3-x}$ ($x = 0$–3), a Sn(II)-system with cubic perovskite structure. Zeitschrift für Naturforschung B, 1978, 33(8): 862–865
2. Weber D. $CH_3NH_3PbX_3$, a Pb(II)-system with cubic perovskite structure. Zeitschrift für Naturforschung B, 1978, 33(12): 1443–1445
3. Mitzi D B. Synthesis, structure, and properties of organic-inorganic perovskites and related materials. In: Progress in Inorganic Chemistry. Karlin K D, ed. John Wiley & Sons: New York, 1999, 48: 1–121
4. Kojima A, Teshima K, Shirai Y, Miyasaka T. Organometal halide perovskites as visible-light sensitizers for photovoltaic cells. Journal of the American Chemical Society, 2009, 131(17): 6050–6051
5. Im J H, Lee C R, Lee J W, Park S W, Park N G. 6.5% efficient perovskite quantum-dot-sensitized solar cell. Nanoscale, 2011, 3 (10): 4088–4093
6. Kim H S, Lee C R, Im J H, Lee K B, Moehl T, Marchioro A, Moon S J, Humphry-Baker R, Yum J H, Moser J E, Grätzel M, Park N G. Lead iodide perovskite sensitized all-solid-state submicron thin film mesoscopic solar cell with efficiency exceeding 9%. Scientific Reports, 2012, 2: 591
7. Lee M M, Teuscher J, Miyasaka T, Murakami T N, Snaith H J. Efficient hybrid solar cells based on meso-superstructured organometal halide perovskites. Science, 2012, 338(6107): 643–647
8. Liu M, Johnston M B, Snaith H J. Efficient planar heterojunction perovskite solar cells by vapour deposition. Nature, 2013, 501 (7467): 395–398
9. Heo J H, Im S H, Noh J H, Mandal T N, Lim C S, Chang J A, Lee Y H, Kim H J, Sarkar A, Nazeeruddin M K, Grätzel M, Seok S I. Efficient inorganic-organic hybrid heterojunction solar cells containing perokskite compund and polymeric hole conductors. Nature Photonics, 2013, 7(6): 486–491
10. Snaith H J. Perovskites: the emergence of a new era for low-cost, high-efficiency solar cells. Journal of Physical Chemistry Letters, 2013, 4(21): 3623–3630
11. Grätzel M. The light and shade of perovskite solar cells. Nature Materials, 2014, 13(9): 838–842
12. Green M A, Ho-Baillie A, Snaith H J. The emergance of perovskite solar cells. Nature Photonics, 2014, 8(7): 506–514
13. Jung H S, Park N G. Perovskite solar cells: from materials to devices. Small, 2015, 11(1): 10–25
14. Xing G, Mathews N, Lim S S, Yantara N, Liu X, Sabba D, Grätzel M, Mhaisalkar S, Sum T C. Low-temperature solution-processed wavelength-tunable perovskites for lasing. Nature Materials, 2014, 13(5): 476–480
15. Dong Q, Fang Y, Shao Y, Mulligan P, Qiu J, Cao L, Huang J. Solar cells. Electron-hole diffusion lengths > 175 μm in solution-grown $CH_3NH_3PbI_3$ single crystals. Science, 2015, 347(6225): 967–970
16. Yakunin S, Sytnyk M, Kriegner D, Shrestha S, Richter M, Matt G J, Azimi H, Brabec C, Stangl J, Kovalenko M V, Heiss W. Detection of X-ray photos by solution-processed lead halide perovskites. Nature Photonics, 2015, 9(7): 444–449
17. Cho H, Jeong S H, Park M H, Kim Y H, Wolf C, Lee C L, Heo J H, Sadhanala A, Myoung N S, Yoo S, Im S H, Friend R H, Lee T W. Overcoming the electroluminescence efficiency limitations of perovskite light-emitting diodes. Science, 2015, 350(6265): 1222–1225
18. Zhao Y, Zhu K. Solution-chemistry engineering toward high-efficiency perovskite solar cells. Journal of Physical Chemistry Letters, 2014, 5(23): 4175–4186
19. Zhou Y, Game O S, Pang S, Padture N P. Microstructures of organometal trihalide perovskites for solar cells: their evolution from solutions and characterization. Journal of Physical Chemistry Letters, 2015, 6(23): 4827–4839
20. Zhou Z, Wang Z, Zhou Y, Pang S, Wang D, Xu H, Liu Z, Padture N P, Cui G. Methylamine-Gas-induced defect-healing behavior of $CH_3NH_3PbI_3$ thin films for perovskite solar cells. Angewandte Chemie International Edition, 2015, 54(33): 9705–9709
21. Quarti C, Grancini G, Mosconi E, Bruno P, Ball J M, Lee M M, Snaith H J, Petrozza A, Angelis F D. The Raman spectrum of the $CH_3NH_3PbI_3$ hybrid perovskite: interplay of theory and experiment. Journal of Physical Chemistry Letters, 2014, 5(2): 279–284
22. Grancini G, Marras S, Prato M, Giannini C, Quarti C, De Angelis F, De Bastiani M, Eperon G E, Snaith H J, Manna L, Petrozza A. The impact of the crystallization process on the structural and optical properties of hybrid perovskite films for photovoltaics. Journal of Physical Chemistry Letters, 2014, 5(21): 3836–3842
23. Brivio F, Frost J M, Skelton J M, Jackson A J, Weber O J, Weller M T, Goni A R, Leguy A M A, Barnes P F F, Walsh A. Lattice dynamics and vibrational spectra of the orthorhombic, tetragonal, and cubic phases of methylammonium lead iodide. Physical Review B: Condensed Matter and Materials Physics, 2015, 92(14): 144308
24. Park B W, Jain S M, Zhang X, Hagfeldt A, Boschloo G, Edvinsson T. Resonance Raman and excitation energy dependent charge transfer mechanism in halide-substituted hybrid perovskite solar cells. ACS Nano, 2015, 9(2): 2088–2101
25. Ledinský M, Löper P, Niesen B, Holovský J, Moon S J, Yum J H, De Wolf S, Fejfar A, Ballif C. Raman spectroscopy of organic-inorganic halide perovskites. Journal of Physical Chemistry Letters, 2015, 6(3): 401–406
26. Vandenabeele P. Practical Raman Spectroscopy: An Introduction. Wiley: New York, 2013
27. Stoumpos C C, Malliakas C D, Kanatzidis M G. Semiconducting tin and lead iodide perovskites with organic cations: phase transitions, high mobilities, and near-infrared photoluminescent properties. Inorganic Chemistry, 2013, 52(15): 9019–9038
28. Kutes Y, Ye L, Zhou Y, Pang S, Huey B D, Padture N P. Direct observation of ferroelectric domains in solution-processed $CH_3NH_3PbI_3$ perovskite thin films. Journal of Physical Chemistry Letters, 2014, 5(19): 3335–3339
29. Kim H S, Im S H, Park N G. Oganolead halide perovskite: new horizons in solar cell research. Journal of Physical Chemistry C, 2014, 118(11): 5615–5625

30. Woodward P M. Octahedral tilting in perovskites: I. geometrical considerations. Acta Crystallographica Section B, Structural Science, 1997, 53(1): 32–43
31. Matsuishi K, Ishihara T, Onari S, Chang Y H, Park C H. Optical properties and structural phase transitions of lead-halide based inorganic-organic 3D and 2D perovskite semiconductors under high pressure. Physics Status Solidi, 2004, 241(14): 3328–3333
32. Maalej A, Abid Y, Kallel A, Daoud A, Lautie A, Romain F. Phase transition and crystal synamics in the cubic perovskite $CH_3NH_3PbCl_3$. Solid State Communications, 1997, 103(5): 279–284
33. Zhou Y, Yang M, Wu W, Vasiliev A L, Zhu K, Padture N P. Room-temperature crystallization of hybrid-perovskite thin films via solvent–solvent extraction for high-performance solar cells. Journal of Materials Chemistry A, Materials for Energy and Sustainability, 2015, 3(15): 8178–8184
34. Yang M, Zhou Y, Zeng Y, Jiang C S, Padture N P, Zhu K. Square‐centimeter solution‐processed planar $CH_3NH_3PbI_3$ perovskite solar cells with efficiency exceeding 15%. Advanced Materials, 2015, 27(41): 6363–6370
35. Hu H, Wang D, Zhou Y, Zhang J, Lv S, Pang S, Chen X, Liu Z, Padture N P, Cui G. Vapour-based processing of hole-conductor-free $CH_3NH_3PbI_3$ perovskite/C_{60} fullerene planar solar cells. RSC Advances, 2014, 4(55): 28964–28967
36. Pisoni A, Jaćimović J, Barišić O S, Spina M, Gaál R, Forró L, Horváth E. Ultra-low thermal conductivity in organic–inorganic hybrid perovskite $CH_3NH_3PbI_3$. Journal of Physical Chemistry Letters, 2014, 5(14): 2488–2492
37. Khilji M Y, Sherman W F, Wilkinson G R. Raman study of three polytypes of PbI_2. Journal of Raman Spectroscopy, 1982, 13(2): 127–133
38. Baleva M, Tuncheva V. Optical characterization of lead monoxide films grown by laser-assisted deposition. Journal of Solid State Chemistry, 1994, 110(1): 36–42

Yuanyuan "Alvin" Zhou is a Ph.D. candidate in the School of Engineering at Brown University with a focus on materials science. He received his B.S. and M.S. degrees in Materials Science and Engineering from Xi'an Jiaotong University. His current research focuses on understanding crystallization mechanisms and fundamental properties of organolead trihalide perovskite, and on developing scalable protocols for high-efficiency perovskite solar cells.

Hector F. Garces is a Research Associate/Research Facility Manager at the Institute for Molecular and Nanoscale Innovation at Brown University. He received his Ph.D. degree in Materials Science from the University of Connecticut (2012), and worked as a postdoctoral research associate at Brown University for about three years. His current research is in synthesis and characterization of perovskite materials for solar cells application, and in processing, characterization, and performance-testing of high-temperature ceramics used as thermal barrier coatings and environmental barrier coatings.

Nitin P. Padture is Professor in the School of Engineering and Director of Institute for Molecular and Nanoscale Innovation at Brown University, since 2012. Prior to 2012, he was College of Engineering Distinguished Professor at the Ohio State University (OSU) for seven years, and also the founding Director of the Materials Research Science & Engineering Center (MRSEC) at OSU. He received his Ph.D. degree from Lehigh University (1991), and he worked as a postdoctoral scholar at the National Institute for Standards and Technology for three years, before serving on the University of Connecticut faculty for ten years. His research interests are in advanced structural ceramics and functional nanomaterials, with applications ranging from jet engines to nanoelectronic devices to solar cells. He has published over 150 referred-journal papers and co-invented 5 patents, which have been cited about 10000 times. A Fellow of the American Ceramic Society, he has received that society's Roland B. Snow, Robert L. Coble, and Richard M. Fulrath awards. He is also a recipient of the US Office of Naval Research Young Investigator award, and he is a Fellow of the American Association for the Advancement of Science. An *alumnus* of the Indian Institute of Technology- Bombay, he has received the Distinguished Service Award from his *alma mater*. He is Editor of the international journal *Scripta Materialia.*